The Role of Vegetation in the Dynamics of West African Monsoons

XINYU ZHENG AND ELFATIH A. B. ELTAHIR

Ralph M. Parsons Laboratory, Massachusetts Institute of Technology, Cambridge, Massachusetts

ABSTRACT

The focus of this paper is the role of meridional distribution of vegetation in the dynamics of monsoons and rainfall over West Africa. A moist zonally symmetric atmospheric model coupled with a simple land surface scheme is developed to investigate these processes. Four primary experiments have been carried out to examine the sensitivity of West African monsoons to perturbations in the meridional distribution of vegetation. In the control experiment, the authors assume a distribution of vegetation that resembles the natural vegetation cover in West Africa. Each perturbation experiment is identical to the control experiment except that a change in vegetation cover is imposed for a latitudinal belt that is 10° in width. The results of the numerical experiments demonstrate that West African monsoons and therefore rainfall distribution depend critically on the location of the vegetation perturbations. Changes in vegetation cover along the border between the Sahara desert and West Africa (desertification) may have a minor impact on the simulated monsoon circulation. However, coastal deforestation may cause the collapse of the monsoon circulation and have a dramatic impact on the regional rainfall. The observed deforestation in West Africa is then likely to be a significant contributor to the observed drought.

1. Introduction

Observations from West Africa indicate a significant decline in rainfall levels since the early 1960s (e.g., Nicholson 1994; Hulme 1994). Nicholson et al. (1996) noted that 1994 was the wettest year since the late 1960s and may represent a break in the multidecadal drought regime. However, observations for 1995 and 1996 suggest continuation of the drought conditions (Horton and Parker 1997). This continuing drought episode spans most of the last three decades with a decline in rainfall levels that is large enough to suggest a significant change in the normal regional climate for this century (Eltahir 1992; Farmer and Wigley 1985). Whether or not this long episode of deficient rainfall will continue remains to be seen. Nevertheless, these observations have motivated many studies on rainfall, droughts, and climate variability over West Africa. Most of these studies can be classified into two groups: studies that emphasize the role of land–atmosphere interaction in the regional climate, and studies that emphasize the role of ocean–atmosphere interaction and sea surface temperature (SST) distribution in the variability of rainfall over West Africa.

First, the studies concerned with the role of land–atmosphere interaction in the variability of regional climate investigate the role of land surface processes that involve vegetation, soil moisture, surface albedo, and evaporation in the dynamics of regional rainfall. The pioneering study on land–atmosphere interaction in this region is that of Charney (1975), which presented a hypothesis for describing the mechanisms of droughts. This hypothesis suggested a significant role for vegetation in the dynamics of rainfall over the Sahel, implying that the rainfall-producing circulation over this region is sensitive to changes in the state of vegetation at the desert border with the Sahara. However, Charney's theory did not address the role of soil moisture and evaporation, which motivated other studies such as Walker and Rowntree (1977) to investigate the effect of soil moisture conditions on circulation and rainfall in West Africa. The role of land surface processes in the regional climate was investigated by several modeling studies: Charney et al. (1975), Charney et al. (1977), Yeh et al. (1984), Sud and Fennessy (1984), Sud and Molod (1988), Cunnington and Rowntree (1986), Kitoh et al. (1988), Rowell and Blondin (1990), Rodriguez-Iturbe et al. (1991), and Xue and Shukla (1993). The role of vegetation and soil moisture in African paleoclimate studies has been emphasized by Kutzbach et al. (1996), where they found that replacing the Sahara desert with grassland and desert soil with more loamy soil could bring their model simulations and paleovegetation observations into closer agreement than otherwise. The results of these studies suggest that the conditions of the land surface as characterized by vegetation cover and soil moisture play a significant role in rainfall vari-

Corresponding author address: Dr. Elfatih A. B. Eltahir, Department of Civil and Environmental Engineering, Massachussets Institute of Technology, Cambridge, MA 02139.
E-mail: eltahir@mit.edu

ability over West Africa. Among those studies on the impact of vegetation cover (e.g., Charney et al. 1975; Xue and Shukla 1993), it is generally concluded that the desertification near the sub-Saharan desert border reduces rainfall within the region of vegetation perturbation and increases rainfall south of the perturbation region. The soil moisture–rainfall interactions are often found to be able to sustain rainfall anomaly and thus provide a positive feedback (e.g., Walker and Rowntree 1977; Yeh et al. 1984; Zheng and Eltahir 1997b).

The second group of studies is concerned with the role of the ocean, and in particular the distribution of SST, in the dynamics of climate over West Africa. The relation of rainfall over this region to the distribution of SST in the tropical Atlantic has been the focus of several studies. At the regional scale, Lamb (1978a,b) and Lamb and Peppler (1992) investigated the relation of Sahel rainfall to the distribution of SST over the Atlantic Ocean. In a similar study, Lough (1986) identified the dominant spatial patterns of normalized SST departures in the tropical Atlantic using principal component analysis and then correlated these different patterns to rainfall in the Sahel region. While most studies are concerned with simultaneous correlation between summer rainfall and summer SST, Druyan (1991) suggested the possibility of predicting summer rainfall based on spring SST patterns. At the global scale, Folland et al. (1986) discussed the relation between Sahel rainfall and worldwide SST distribution. The use of SST observations for the purpose of forecasting rainfall in the Sahel was explored by Owen and Ward (1989) using a global SST dataset. The results of all these studies suggest that the conditions over the Atlantic Ocean as characterized by SST may play a significant role in rainfall variability over West Africa.

A different view on the mechanisms of floods and droughts over West Africa has been proposed recently by Eltahir and Gong (1996). They suggested that rainfall variability over this region is a manifestation of a large-scale ocean–atmosphere–land interaction. According to this theory, dynamics of wet and dry years over West Africa are governed by not only the land–atmosphere interaction, or the ocean–atmosphere interaction considered independently, but the critical factor to consider is the meridional gradient of boundary layer conditions between the land region and the Atlantic Ocean. The measure that was proposed to describe these conditions over land and the ocean is the meridional gradient of moist entropy (or moist static energy). This theory predicts that a flat meridional distribution of entropy does not drive any circulation and that a relatively large gradient of entropy should drive a strong monsoon circulation, which is of course the main rainfall-producing system in the Sahel region.

The study of Eltahir and Gong (1996) builds on the results of the earlier studies on the dynamics of zonally symmetric thermally direct atmospheric circulations by Held and Hou (1980), Lindzen and Hou (1988), and, in particular, Plumb and Hou (1992) and Emanuel (1995). In short, for a meridional circulation to develop over any tropical region off the equator, the absolute vorticity near the tropopause has to reach a threshold value of zero. However, for a moist atmosphere that satisfies a quasi-equilibrium balance between moist convection and the radiative forcing, the absolute vorticity at upper-tropospheric levels is a function of latitude and the meridional distribution of boundary layer entropy. Hence, the onset of a monsoon circulation depends in a nonlinear fashion on these two factors. Eltahir and Gong (1996) argued that the location of the region of West Africa, relatively close to the equator, dictates that the dynamics of monsoon over the region are relatively sensitive to interannual fluctuations in the meridional gradient of boundary layer entropy. They further presented observations on entropy and wind over West Africa during the monsoon seasons of relatively wet year of 1958 and relatively dry year of 1960. These observations are consistent with the proposed relation between boundary layer entropy and the monsoon circulation: a large meridional gradient of boundary layer entropy, a healthy monsoon, and relatively wet conditions over the Sahel region were observed in 1958; a nearly flat distribution of entropy, very weak circulation, and relatively dry conditions were observed in 1960.

The theory of Eltahir and Gong (1996) is consistent with the empirical observations of sea surface temperature anomalies (SSTAs) in the tropical Atlantic and rainfall in the Sahel region (Lamb 1978a,b; Lough 1986). Theoretically, a cold (warm) SSTA in the region located south of the West African coast should favor a large (small) meridional gradient of entropy, a strong (weak) monsoon circulation, and wet (dry) conditions in the Sahel. A large body of observations confirms that cold (warm) SSTAs off the southern coast of West Africa are associated with wet (dry) years in the Sahel region (Lamb 1978a,b; Lough 1986). However, the gradient of entropy is also controlled by the corresponding boundary layer conditions over land. In particular, the role of vegetation in sustaining large-scale tropical circulations was investigated by Eltahir (1996). He presented observational and numerical evidence that tropical deforestation reduces the total net surface radiation and therefore total surface heat flux, including sensible and latent forms. Hence, large-scale deforestation reduces boundary layer entropy relative to the surroundings and results in weakening of tropical circulations. Applying these general concepts to West African monsoons, we expect that the tropical West African deforestation will leave a significant signature in the meridional distributions of net surface radiation, total surface heat flux, and boundary layer entropy. Since the gradient of boundary layer entropy is closely related to the strength of monsoons, West African deforestation is then likely to cause changes of monsoon circulations.

In this paper, we simulate and compare the response of the monsoon circulation to changes in the vegetation

distribution considering several different scenarios: degradation of land cover along the northern border between West Africa and the Sahara desert (desertification), and degradation of land cover along the southern coast of West Africa (deforestation). While the desertification scenario is similar to the changes in land cover that were assumed by several previous studies (e.g., Charney 1975; Charney et al. 1977; Xue and Shukla 1993), the sensitivity of rainfall in West Africa to deforestation along the coast has not yet received a similar level of attention. Zheng and Eltahir (1997a) reported some preliminary results regarding the relative importance of tropical deforestation and sub-Saharan desertification. However, this paper presents a more detailed and complete analysis of the issue.

We first discuss the applicability of a zonally symmetric model to West African monsoons. A zonally symmetric model of the monsoon circulation is presented in section 3. Then, a study on the sensitivity of West African monsoons to desertification and deforestation is described in section 4, followed by a discussion in section 5. The final section of the paper summarizes our conclusions.

2. The assumption of zonal symmetry for studying West African monsoons

In the literature, a few studies use zonally symmetric or zonally averaged models to study West African monsoons. Most notably, the pioneering work of Charney (1975) used an analytical zonally symmetric model to study the qualitative effect of increasing surface albedo on Sahelian rainfall. Xue et al. (1990) investigated the impact of sub-Saharan desertification on West African rainfall using a zonally averaged model of the West African monsoon. Their justification for using a two-dimensional model is based on the fact that West Africa has a zonally uniform distribution of rainfall, vegetation, and other meteorological quantities. No quantitative analyses were presented in both of these studies to support this assumption. Here we assess the effect of ignoring zonal asymmetries, by looking at the water vapor and moist static energy budget for the region of West Africa, for the climatological conditions.

a. Water vapor

We use the monthly mean data from the National Centers for Environmental Prediction (NCEP), for the 1982–94 climatology (Kalnay et al. 1996). West Africa is defined here as the region from 5° to 20°N, 15°W to 15°E, as sketched in Fig. 1.

According to Newell et al. (1972a), the water vapor conservation can be expressed as

$$\frac{\partial W}{\partial t} + \nabla \cdot Q = E - P, \qquad (1)$$

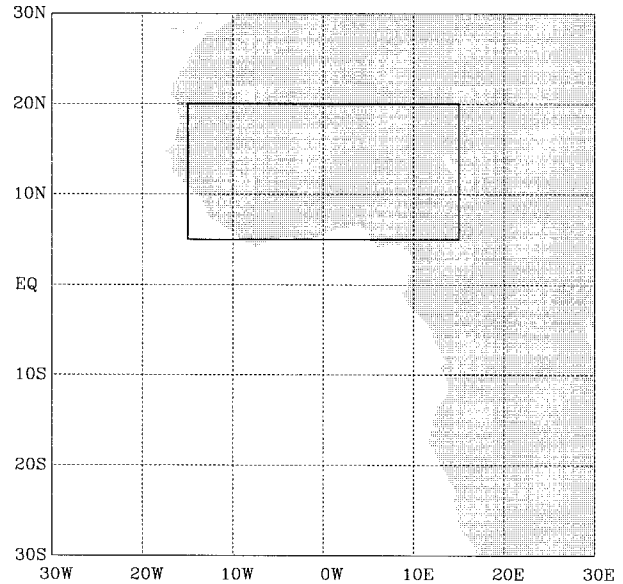where $W = (1/g) \int_{p_u}^{p_s} q \, dp$ is precipitable water, p_s surface

FIG. 1. Map of West Africa and the region of the study, defined as the region from 5° to 20°N, 15°W to 15°E (the dark rectangle).

pressure, and p_u the pressure above which the flux and flux convergence become negligible (here it is taken as 300 mb); $Q = iQ_\lambda + jQ_\phi$, where i, j are eastward and northward pointing unit vector, respectively. Here the total zonal flux of water vapor Q_λ is defined as

$$Q_\lambda = \frac{1}{g} \int_{p_u}^{p_s} qu \, dp, \qquad (2)$$

and the total meridional flux of water vapor Q_ϕ is

$$Q_\phi = \frac{1}{g} \int_{p_u}^{p_s} qv \, dp. \qquad (3)$$

The monthly averaged fluxes of water vapor can then be expressed as

$$\overline{Q}_\lambda = \frac{1}{g} \int_{p_u}^{p_s} (\overline{q}\,\overline{u} + \overline{q'u'}) \, dp \qquad (4)$$

and

$$\overline{Q}_\phi = \frac{1}{g} \int_{p_u}^{p_s} (\overline{q}\,\overline{v} + \overline{q'v'}) \, dp, \qquad (5)$$

where overbars indicate the monthly mean values; primes indicate the transient eddies. As demonstrated by Flohn et al. (1965) and Rasmussen (1972), over West Africa in summer, the total water vapor fluxes are dominated by the monthly mean winds, with transient eddy fluxes an order of magnitude smaller. Therefore, we can approximately calculate the water vapor fluxes using monthly mean winds, a procedure also used by Kidson (1977).

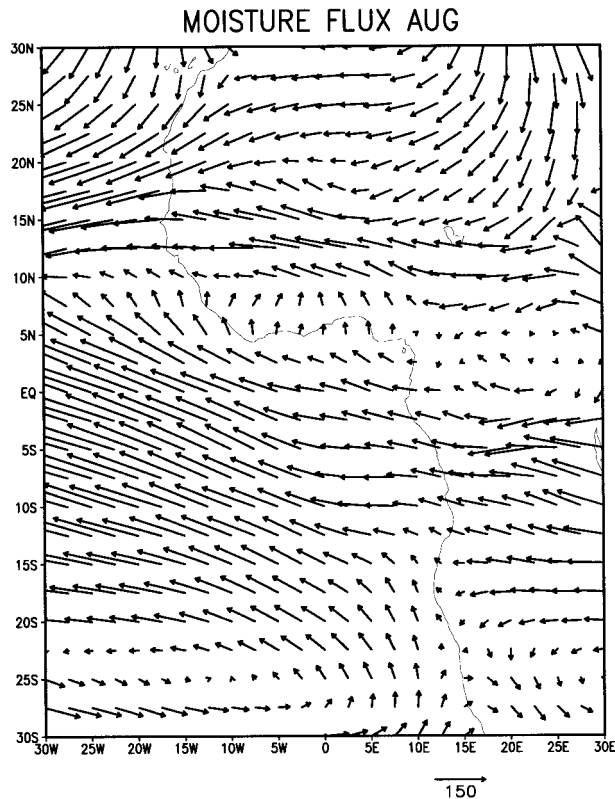For the region of this study, which is sketched by the

MOISTURE FLUX AUG

FIG. 2. The vertically integrated water vapor fluxes (Q_λ, Q_ϕ) in August (unit: kg m^{-1} s^{-1}).

dark rectangle in Fig. 1, the net water vapor convergence can be expressed, through application of the Gauss theorem as $(F_x + F_y)/A$, where F_x is the amount of net water vapor flux across eastern–western boundaries, F_y is the amount of net water vapor flux across northern–southern boundaries (the unit of F_x and F_y is kg s^{-1}), and A is the area of the region. Here, A can be calculated by

$$A = a^2 \Delta\lambda(\sin\phi_2 - \sin\phi_1), \qquad (6)$$

where $\Delta\lambda = \pi/6$, which is the longitude difference between the eastern and the western boundaries in radians; $\phi_1 = 5°N$ (southern boundary) and $\phi_2 = 20°N$ (northern boundary); and a is the earth's radius. The water vapor fluxes in August are shown in Fig. 2. The magnitude of zonal fluxes is in general larger than that of meridional fluxes. This is because the zonal wind is much larger than the meridional wind in terms of the magnitude. In addition to that, the zonal fluxes show prevailing westward transport of moisture in most of the regions except the region of strong monsoon southwesterlies, between around 5° and 10°N. In the mean time, the meridional fluxes show northward transport by the monsoon southwesterlies from the tropical Atlantic Ocean to the West African region. The qualitative features of water vapor transport agree well with the

study of Kidson (1977) in which he showed that streamlines of the water vapor flux are fairly zonal.

However, the more meaningful quantity to look at is the water vapor convergence for the region of our study since it is the moisture convergence that is associated with vertical motions and therefore rainfall. In order to be able to apply zonally symmetric models to study West African monsoons, the net zonal water vapor flux F_x (magnitude) must be substantially smaller than the net meridional water vapor flux F_y (magnitude), during the summer months. In other words, the total net water vapor flux within the region ($F_x + F_y$) must be dominated by F_y. The seasonal variations of F_x, F_y, and ($F_x + F_y$), scaled by the area of the region of our study A [Eq. (6)], are shown by Fig. 3a. The positive values indicate net water vapor into the region and negative values indicate net water vapor out of the region. It is clear that the net meridional fluxes are dominant over the zonal fluxes in summer (July–September). The zonal water vapor flux convergence (F_x) is negative over most of the summer. This suggests that the zonal asymmetries contribute a net water vapor flux out of the region. Compared to the net meridional water vapor flux (F_y) in the region, the effect of zonal asymmetries on the water vapor flux convergence is secondary. In particular, in August and September when the rainfall reaches its maximum in the Sahel, the contribution of F_x to the total net water vapor flux is less than around 30%.

In summary, from the standpoint of water vapor convergence in West Africa, the effect of north–south water vapor flux convergence is dominant. In fact, during summer months, the net meridional flux of water vapor injects moisture into the West African region. At the same time, the net zonal flux of water vapor brings moisture out of the region with substantially smaller magnitude. This study agrees with Lamb (1983) and Gong and Eltahir (1996), where it was concluded that the evaporation over the tropical Atlantic Ocean is a primary moisture source for the West African monsoon.

b. Moist static energy

We now examine the effect of neglecting zonal asymmetries on moist static energy, which has been shown to be a crucial quantity in moist atmospheres (Emanuel 1994; Emanuel et al. 1994). Similar to our analysis of water vapor, the monthly averaged vertically averaged zonal flux of moist static energy ($\overline{M}_\lambda$) can be approximated by

$$\overline{M}_\lambda = \frac{1}{g} \int_{p_u}^{p_s} (C_p \overline{T} + L_v \overline{q})\overline{u} \, dp, \qquad (7)$$

where the contribution from transient eddies has been ignored (Newell et al. 1972b); L_v is latent heat of vaporization. The vertically averaged meridional flux of moist static energy ($\overline{M}_\phi$) is
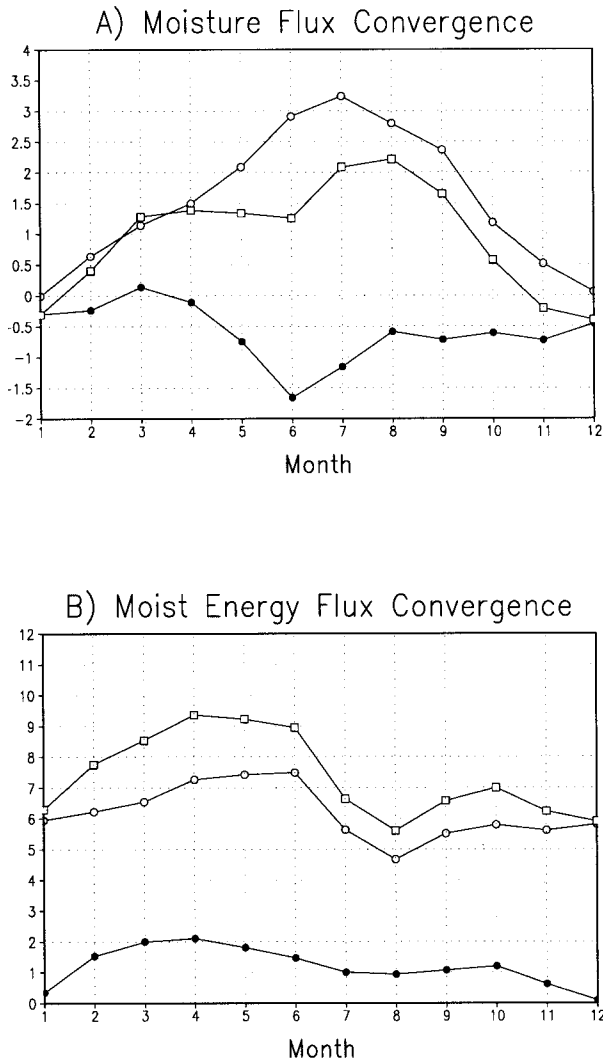
A) Moisture Flux Convergence

B) Moist Energy Flux Convergence

FIG. 3. The seasonal evolution of the vertically integrated (a) net water fluxes (unit: 10^{-5} kg m^{-2} s^{-1}), and (b) net moist static energy fluxes (unit: 10^3 W m^{-2}), scaled by the area of the region A, which can be calculated by Eq. (6). The bullets indicate the net flux across the eastern–western boundaries (F_x); the circles the net flux across northern–southern boundaries (F_y); the squares the total net fluxes. Positive values mean the net flux convergence; negative values mean the net flux divergence.

$$\overline{M}_\phi = \frac{1}{g} \int_{p_u}^{p_s} (C_p \overline{T} + L_v \overline{q}) \overline{v} \, dp. \qquad (8)$$

For the region of our study, the time evolution of net moist static energy fluxes are shown in Fig. 3b. Again, we see that during summer months, the meridional flux convergence is dominant over the zonal flux convergence.

By analyzing the effect of zonal asymmetries for the region of West Africa, in terms of moisture and moist static energy convergence, we found that the error caused by neglecting zonal asymmetries is relatively small. Zheng (1997) also analyzed the net convergence

of angular momentum in West Africa. He found that the effect of zonal asymmetries on angular momentum is also negligible. Therefore, for the West African region, a zonally symmetric model should be sufficient to describe the gross features of seasonal rainfall variability, as long as we are not interested in individual synoptic disturbances, which have to be modeled using a three-dimensional model. In what follows, the framework of zonal symmetry will be applied to West African monsoons. Our focus is to understand physical mechanisms using a zonally symmetric model.

3. Model description

The model used in this study is a moist and zonally symmetric model. The model equations include primitive momentum equations, the thermodynamic equation, the water vapor equation and the mass continuity equation. The hydrostatic approximation has been applied. The model is designed specifically to study the dynamics of monsoons and was not designed as a climate model. Hence, the philosophy in building this tool is different from that of climate models; a limited set of essential processes is included in order to study and define the critical processes that are important for simulating realistic monsoons.

The observations show that the vegetation, temperature, specific humidity, and rainfall in West Africa are approximately uniform in the zonal direction; our analyses in section 2 demonstrated that a zonally symmetric model should be capable of simulating the essential features of West African monsoons. The model represents the zonal average between 15°W and 15°E. The model domain is global horizontally and extends from surface up to 25 km (log pressure) vertically. The grid points are evenly spaced in sine latitude horizontally with 60 increments (about 2.0° resolution in latitude in the Tropics) and also equally spaced vertically with 25 increments (1-km vertical resolution). The time integration scheme is semi-implicit and the time step is 20 min. The standard diffusion used in these experiments is fourth order in the horizontal and conventional Fickian diffusion in the vertical. In addition, the diffusion scheme is designed in such a way that the decay timescale of the two-grid-length waves in the horizontal is comparable with the decay timescale of the two-grid-length waves in the vertical. In this paper, the latter is half the former. The diffusion coefficient is 5 m^2 s^{-1}. The following is a brief description of the model physical processes.

a. Moist convection

The effect of moist convection on large-scale flows is parameterized using the Emanuel scheme (Emanuel 1991), which is a physically based scheme taking account of current available theories, observations, and numerical simulations. The version we use is version

2.02. Based on observations of inhomogeneity of individual convective clouds, the basic assumption of this scheme is that the fundamental entities in convection are those subcloud-scale [O (100 m)] drafts rather than the clouds themselves. The main closure parameters are parcel precipitation efficiency, ϵ^i, which determines the fraction of condensed water in a parcel lifted to level i that is converted to precipitation; the fraction σ_i^s of precipitation that falls through unsaturated air; and σ_d, which is the fraction area covered by the precipitating downdrafts. These represent the physical processes responsible for determining how much condensed water reevaporates, thus moistening and cooling the air, and how much falls out of the system, leading to warming and drying. Thus, this scheme directly relates the large-scale temperature and moisture tendencies to microphysical parameters. The scheme is able to handle both deep and shallow convections.

The level of humidity is checked after each time step. If the atmosphere is supersaturated, the excess water vapor is eliminated by large-scale precipitation without reevaporation. The whole process is constrained by the conservation of enthalpy.

b. Radiation

We use a fast radiation parameterization scheme developed by Chou et al. (1991). The scheme combines both longwave and shortwave radiation to produce a computationally fast yet still accurate radiation parameterization.

For longwave absorption, this scheme uses the Chou (1984) broadband transmission approach for water vapor, the Chou and Peng (1983) method for carbon dioxide, and the Rodgers (1968) method for ozone. The scheme includes the water vapor line and continuum absorption, carbon dioxide absorption through band centers and band wing regions, and infrared ozone-absorption bands.

Solar radiation is absorbed by water vapor and ozone, scattered by cloud droplets, and reflected at the surface. The scheme employs the parameterization method of Lacis and Hansen (1974) for ozone and water vapor. Plane-parallel clouds (modeled with a delta-Eddington two-stream flux model) (King and Harshvardhan 1985; Joseph et al. 1976) provide fractional coverage. For all the experiments we have described in this article, we assume clear-sky condition and no clouds included in the radiation code. The cloud–radiation feedback will be included in the next level of model development. We will discuss the effect of neglecting cloud–radiation feedback in section 6.

The model top is at 25 km (about 38.8 mb) and the surface is at 1000 mb. For the radiation calculation, above the model top, we add nine layers up to 1 mb in radiative equilibrium. The carbon dioxide concentration is 330 ppm. Ozone mixing ratio and stratospheric water vapor profile are from the Air Force Geophysics Laboratories standard atmosphere (McClatchey et al. 1972).

c. Surface scheme

The surface configuration is as follows: the continental edge is located at 5°N mimicking the southern coast of West Africa; north of it is land, whereas south of it is ocean. The ocean temperature is specified from the observation, as will be discussed later in more detail. The surface albedo for ocean surface is 0.10. The land surface temperature is computed using the energy balance and assuming zero heat capacity.

We use the Budyko dryness index as an indicator of vegetation type (Budyko 1974). According to Budyko (1974), for tropical forest D is generally less than 1.0 whereas for the desert region D is above 3.0. The savanna region D lies between 1.0 to 2.0. The semidesert region D is from 2.0 to 3.0. In our land surface scheme, we follow Gutman et al. (1984) in relating the index of dryness (D) with both surface albedo (α) and surface water availability (w) as follows:

$$w = 1.23\frac{\tanh D}{D} - 0.33 \qquad D \geq 0 \qquad (9)$$

and

$$\alpha = \begin{cases} \min(0.25,\ 0.07 + 0.06D) & D \geq 1, \\ 0.10 & 0 < D < 1. \end{cases} \qquad (10)$$

Note that within the tropical forest region (defined as $0 < D < 1$) there is no dependence of the surface albedo on the dryness index. On the other hand, the upper limit of the surface albedo is set to 0.25, which is reasonable for deserts. The surface water availability is prescribed to be close to 1.0 (moist surface) in the forest region and approaches 0.0 as D increases in the desert and semidesert regions. Surface fluxes are parameterized by the bulk aerodynamic formulas.

This simple land surface scheme basically uses the dryness index D as an indicator of vegetation types. A distribution of D corresponds to a particular vegetation distribution, giving us a unique distribution of surface albedo and a unique distribution of water availability. Hence, for a given vegetation distribution we know how much of the solar insolation is absorbed at the surface (through surface albedo) and how much the surface net radiation is partitioned between latent heat flux and sensible heat flux. This is done through water availability w. The actual evaporation is defined as $w \times E_p$, where E_p is the potential surface evaporation calculated by the bulk formulas. It should be pointed out that we did not include any of the dynamics of the surface hydrology in this model. This is because we are mainly concerned with perpetual summer equilibrium states under different vegetation patterns. However, in Zheng (1997), we extend the model by including seasonal solar forcing
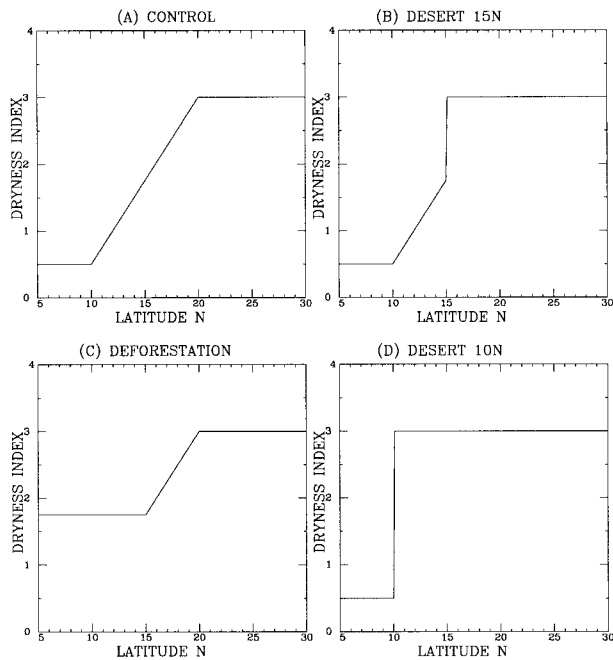
FIG. 4. The distribution of vegetation (described by the dryness index) for (a) the control experiment, (b) the desertification (from 15°N) experiment, (c) the deforestation experiment, and (d) the desertification (from 10°N) experiment.
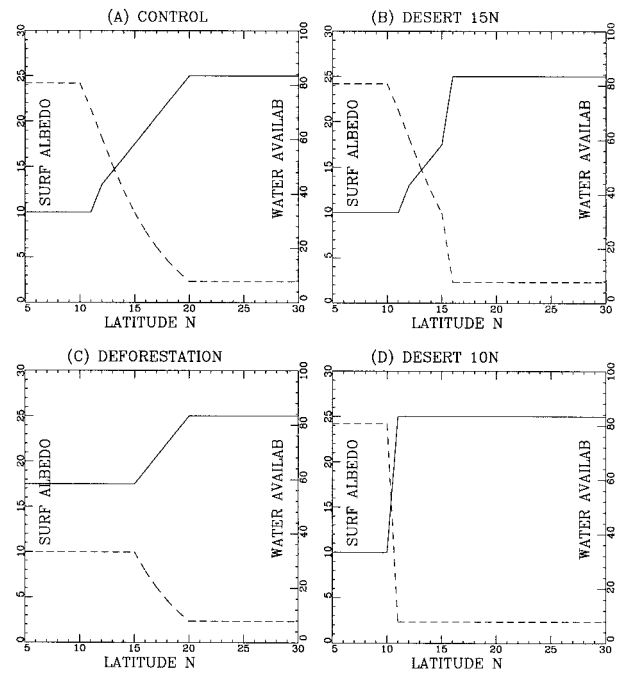

FIG. 5. The distributions of surface albedo (solid) and water availability (dashed) (in percentage) for (a) the control experiment, (b) the desertification (from 15°N) experiment, (c) the deforestation experiment, and (d) the desertification (from 10°N) experiment. The scale on the left-hand side y axis is for surface albedo, and the scale on the right-hand side y axis is for water availability.

and soil hydrology, the main results are not influenced significantly.

4. Sensitivity of the West African monsoon to the meridional distribution of vegetation

In the previous sections we argued that the dynamics of monsoons are regulated by the meridional distribution of boundary layer entropy. Since any change of land cover is necessarily associated with changes in surface albedo, surface water availability (root zone depth), as well as surface roughness, the net surface radiative flux and the entropy flux from the underlying surface will change correspondingly (Eltahir 1996). Therefore, any land cover transformation is likely to have substantial effect on boundary layer entropy and thus the monsoon circulation. Here, we would like to investigate this issue and test the sensitivity of West African monsoons to changes in vegetation that may occur at different latitudinal belts. Our approach consists of numerical experiments using the model that has been described in the previous section. Four primary experiments were performed and will be described in the following sections.

a. Control experiment

The natural vegetation in West Africa ranges from short grass at the desert border to humid rain forests at the southern border of the region near the Atlantic coast.

The area in between is occupied by several vegetation zones ranging from tropical forests, to woodland, savanna, shrubs, and short grass. The vegetation pattern in terms of the index of dryness (D) for the control experiment is specified in Fig. 4a. Also in Fig. 4 we show the vegetation perturbations that will be discussed later. For the area between the coast (5°N) to 10°N, we assign a D value of 0.50, which corresponds to tropical forests; north of 20°N, D is set to 3.0, implying a surface albedo of 0.25, which corresponds to desert conditions. The dryness index is assumed to increase linearly between 10° and 20°N to represent the transition from the tropical forest conditions to the desert conditions. The corresponding patterns of surface albedo and water availability are described in Fig. 5.

For the sake of simplicity, we are going to concentrate on the perpetual summer case. The solar insolation of 15 August is assumed in these experiments; this date coincides approximately with the period of the observed maximum precipitation in the Sahel region. The oceanic temperature is specified as the observed mean SST distribution in August (climatology 1981–94, averaged from 5°W to 5°E) off the West African coast (Reynolds and Smith 1994). The model is integrated for 500 days to achieve a quasi-steady state. Hence, the numerical simulations discussed here describe the steady-state solutions for the dynamics of monsoons that correspond
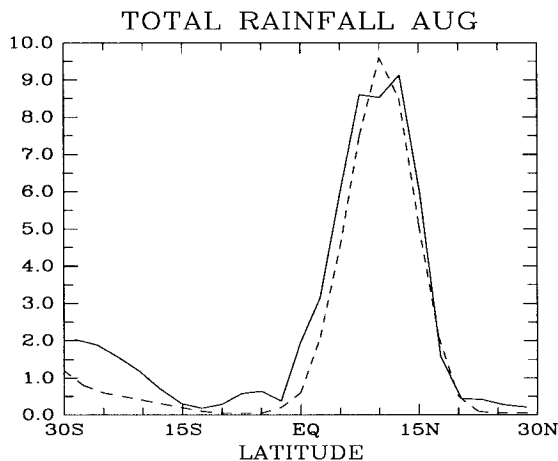
TOTAL RAINFALL AUG

FIG. 6. The August rainfall meridional profiles of the model control experiment with seasonal cycle (solid) and the observed GPCP 1987–94 climatology averaged from 15°W to 15°E, in mm day^{-1}.

to different surface boundary conditions, but using the same solar forcing.

The results of the control experiment indicate a development of a healthy monsoon circulation. A detailed comparison between the model control experiment (with seasonal cycle) and the NCEP reanalysis data is given in the appendix. Note that the control experiment we describe here cannot be compared with the observed August rainfall exactly (where August is just part of the seasonal cycle). Zheng (1997) compared the results from the same model with seasonal cycle to the observations. The model rainfall in August agrees reasonably well with that of the Global Precipitation Climatology Project (GPCP) rainfall data (Huffman et al. 1995), in terms of the location of maximum rainfall (ITCZ) and the north–south gradient of the rainfall (Fig. 6). Furthermore, similar perturbation experiments have been performed with seasonally varying radiative forcing. The qualitative results are not influenced. Therefore, this paper only discusses results from our steady-state model experiments.

Figure 7a shows the distribution of absolute and planetary vorticities at the tropopause. While the inviscid theory predicts zero absolute vorticity at the tropopause, the model shows effective weakening of the absolute vorticity from about 25°S to 15°N. A slight nonconservation of angular momentum is implied by nonzero absolute vorticity within the region, presumably due to the inclusion of the numerical diffusion. The meridional distributions of total rainfall, evaporation, and $P - E$ (P total rainfall, E evaporation; this is a measure of large-scale moisture convergence) are shown in Figs. 8, 9, and 10, respectively. The maximum precipitation occurs at a latitude between 12° and 13°N where $P - E$ also maximizes.

Notice that for our steady-state experiment here, the location of the ITCZ is not very far from the reality ($\sim$10°–12°N). The latitude of the maximum evaporation (Fig. 9), however, is south of the ITCZ at around 8°–

10°N. This is due to larger surface water availability near the coastal region as shown in Fig. 5. The meridional distribution of boundary layer entropy is shown in Fig. 11. Note that the latitude of maximum boundary layer entropy (about 22°N) is far north of the latitude of maximum rainfall. The latitude of maximum boundary layer entropy can be viewed as the northern boundary of the monsoon circulation since this is where angular momentum contour becomes vertical (Emanuel 1995). In addition, the results that are not presented here show a strong easterly jet at upper levels and a surface westerly flow over the land. The same results show westerly jets in both hemispheres with a much stronger winter jet. The intensity of these jets is unrealistically strong since we use a zonally symmetric model. In reality, midlatitudinal eddies would tend to reduce the intensity of these jets. Overall, these features are consistent with the development of a healthy monsoon (Ramage 1971).

b. Desertification (from 15°N) experiment

This experiment is identical to the control experiment except that the vegetation cover in the region between 15° and 20°N is removed resulting in expansion of the desert (see Fig. 4b). This change in the surface boundary mimics the desertification of the semiarid region that is located to the south of the Sahara desert and is similar to the case considered by Charney (1975) and several other studies.

Even with the desertification in the semiarid region, the monsoon circulation still exists and is strong. This can be inferred from Fig. 10. The distribution of upper-level absolute vorticity in Fig. 7b indicates that the north edge (about 12°N) of the weakened absolute vorticity region is slightly south of the corresponding location of the control experiment. The latitudinal profile of rainfall in Fig. 8 shows that the rainfall decreases substantially within the perturbation region (from 15° to 20°N). This is due to both the decrease of moisture convergence and the decrease of the local evaporation. However, south of 15°N, rainfall even increases. The increase of rainfall south of the perturbation region is mainly associated with the increase of the large-scale moisture convergence, which is consistent with the stronger and more concentrated monsoon updraft, as can be seen from Fig. 10. Furthermore, the location of the maximum rainfall, and hence the ITCZ, does not change significantly following the desertification (Fig. 8). The ITCZ seems to be more concentrated following the desertification. A surface westerly wind (not shown) also develops over the land with similar magnitude to that of the control case. In summary, desertification near the southern edge of the desert reduces the rainfall within the desertification region and enhances the rainfall south of it. However, the resulting modification of the circulation is not significant enough for the monsoon to collapse.
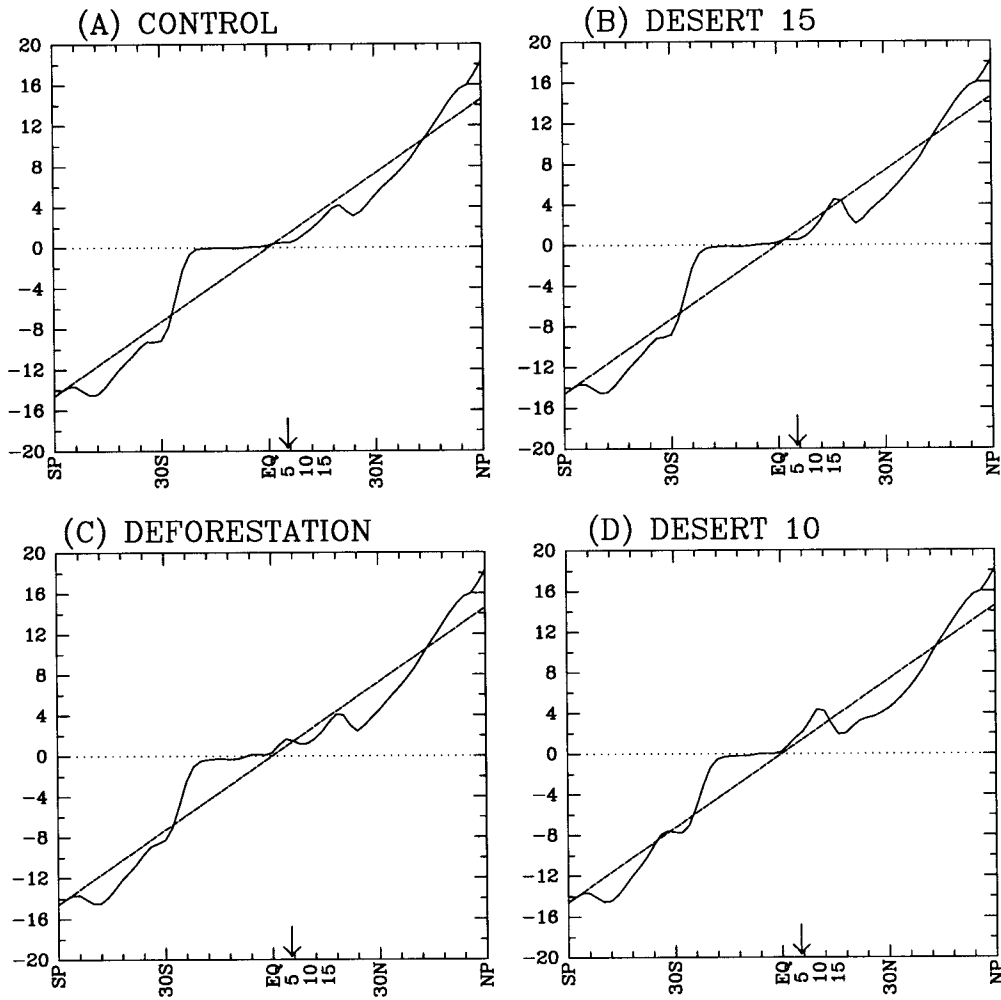
FIG. 7. The absolute (solid) and planetary (dashed) vorticities (unit: 10^{-5} s^{-1}) at the tropopause for (a) control, (b) desertification (from 15°N), (c) deforestation, and (d) desertification (from 10°N). The vertical arrow indicates the coastline of the southern Atlantic Ocean.
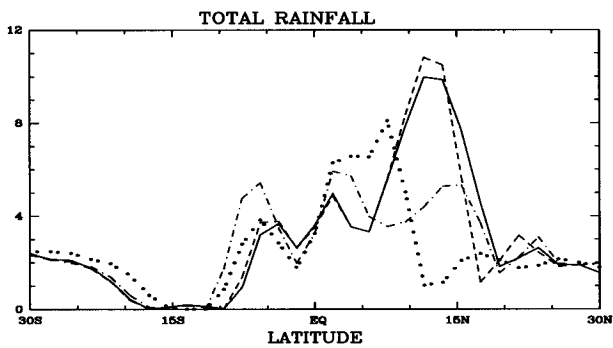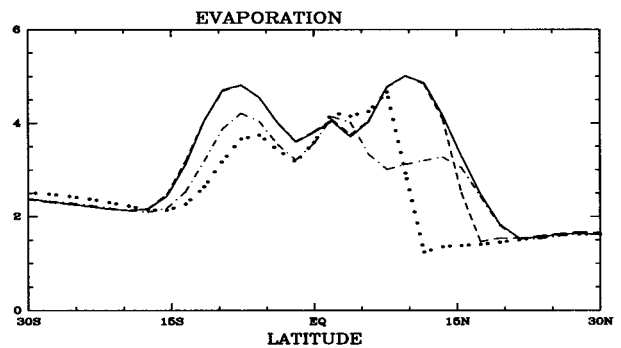

FIG. 8. The meridional distribution of rainfall in (mm day^{-1}), for the control (solid line), desertification from 15°N (dashed line), deforestation (dashed–dotted line), and desertification from 10°N (dotted line).
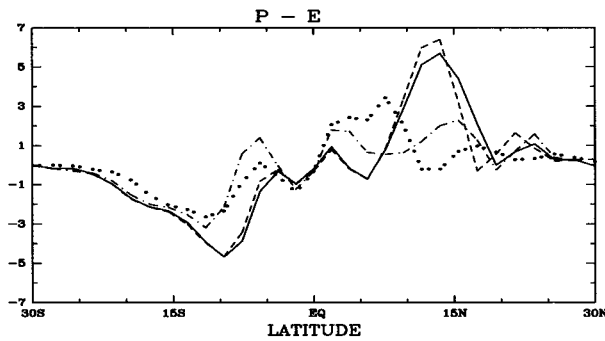
FIG. 9. The meridional distribution of evaporation in (mm day^{-1}), for the control (solid line), desertification from 15°N (dashed line), deforestation (dashed–dotted line), and desertification from 10°N (dotted line).

FIG. 10. The meridional distribution of the difference between precipitation and evaporation ($P - E$) in (mm day^{-1}) for the control (solid line), desertification from 15°N (dashed line), deforestation (dashed–dotted line), and desertification from 10°N (dotted line).

FIG. 12. The total net surface radiation (W m^{-2}) for the control (solid line), desertification (from 15°N, dashed line), deforestation (dashed–dotted line), and desertification (from 10°N, dotted line).

c. Deforestation experiment

This experiment is identical to the control case except that the vegetation cover for the region 5°–15°N is replaced by savanna with the dryness index value at 15°N (see Fig. 4c). In the control experiment, this region is covered by tropical forest between 5° and 10°N and by savanna for the subregion between 10° and 15°N. This experiment attempts to simulate the worst-case scenario for tropical deforestation in West Africa.

Unlike the desertification experiment, the influence of deforestation is dramatic. The maximum rainfall (~5 mm day^{-1}) is only half of the rainfall maximum in the control experiment (Fig. 8). In addition, the moisture convergence (which is a measure of the strength of the monsoon circulation) is only one-third of the value in the control case, implying a much weaker circulation (Fig. 10). In accordance with this, the upper-level absolute vorticity is no longer close to zero over the land (Fig. 7c), indicating the collapse of the nonlinear monsoon circulation. The collapse of the monsoon can be explained as follows. Figure 12 shows the net surface radiative fluxes (by convention, downward fluxes are defined as positive, upward fluxes are defined as negative). It is clear that within the perturbation region the
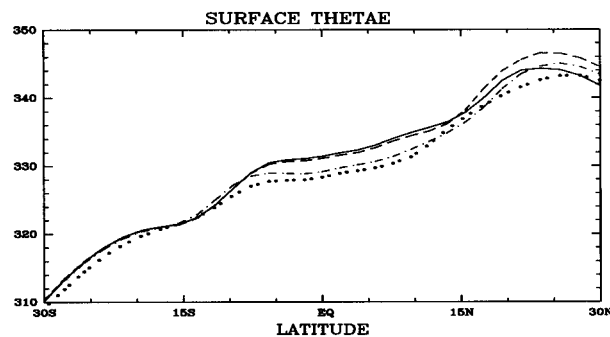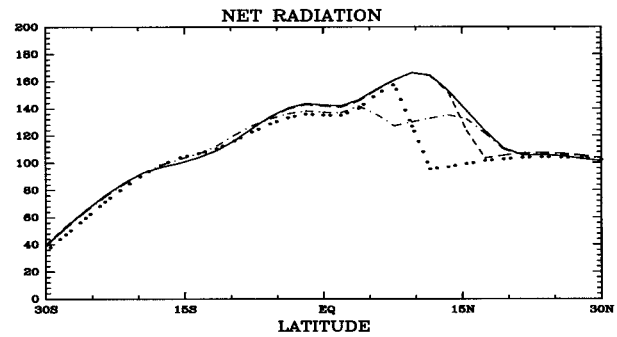
net radiative flux is much smaller than that of the control case (about 40 W m^{-2}). In general, the degradation of the vegetation cover will induce an increase of albedo and a decrease of surface water availability (Fig. 5). The increase of the surface albedo will decrease the surface solar (shortwave) radiative flux. On the other hand, the decrease of the surface water availability has the tendency of heating up the land surface. This results in larger outgoing longwave radiative flux (other things being the same). In addition, the decrease of the surface water availability also reduces the surface evaporation (Fig. 9). This introduces less water vapor into the atmosphere and a smaller greenhouse effect. The combination of the two effects induced by smaller surface water availability produces a decrease of the net longwave radiative flux. To confirm this reasoning, we here show the surface net shortwave radiative flux and the net longwave radiative flux for the four standard experiments (Figs. 13 and 14). For the case of deforestation, we see that both shortwave and longwave components contribute to the decreased net surface radiation comparably. Therefore, the overall effects of both shortwave and longwave radiative components arising from the degradation of the vegetation cover lead to a significant decrease of the net surface radiation. This reduction in net surface radiation results in a similar reduction of surface entropy flux in the coastal region,

FIG. 11. Boundary layer entropy in terms of surface θ_e in kelvins for the control (solid line), desertification from 15°N (dashed line), deforestation (dashed–dotted line), and desertification from 10°N (dotted line).
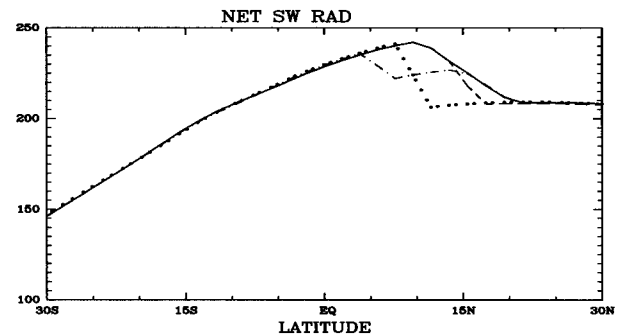

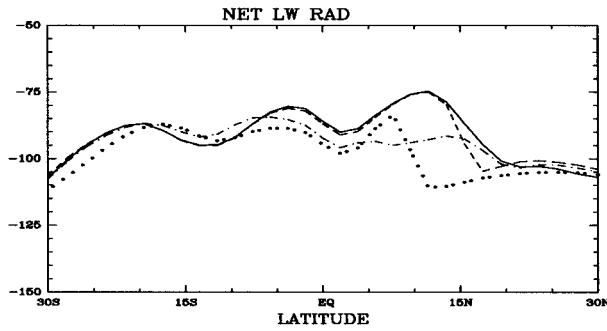FIG. 13. Same as Fig. 12 except for net surface shortwave radiative flux.

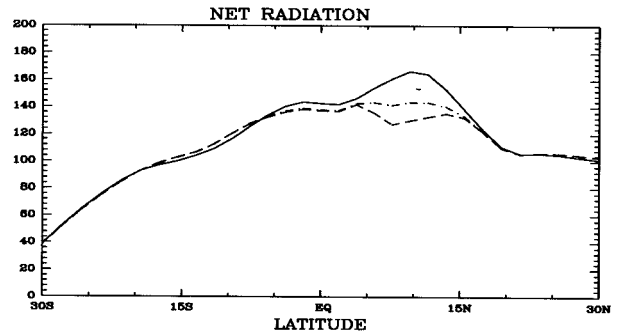FIG. 14. Same as Fig. 12 except for net surface longwave radiative flux.

FIG. 16. The surface net radiation (W m^{-2}) for the control (solid line), deforestation (dashed line), and the experiment with the same surface albedo as the deforestation experiment and the same surface water availability as the control case (dashed–dotted line).

hence reducing substantially the boundary layer entropy there. The total surface heat flux (including sensible and latent forms), which equals the net radiative flux over the land, is displayed in Fig. 15. The reduction of the surface heat flux over the land results in the reduction of boundary layer entropy in the coastal region and therefore the contrast between the coastal land and ocean is too weak to trigger a monsoon circulation (Fig. 11). Therefore, the monsoon collapses.

Note also that the change of boundary layer entropy is not limited within the region of perturbation. This is because the initial local change of boundary layer entropy due to vegetation perturbation affects the strength of monsoon circulation, which in turn tends to modify the boundary layer entropy within the region of deep convection where the atmosphere is relatively well mixed (Emanuel 1995). For the region of strong subsidence (Southern Hemisphere Tropics and subtropics), the boundary layer is decoupled with the free atmosphere and the boundary layer entropy there is not influenced by the imposed vegetation perturbation significantly. Figure 11 clearly shows that the boundary layer entropy has a substantial reduction within the deep convective region following the deforestation, associating with substantial change of monsoon circulation we described earlier. On the other hand, the desertification (from 15°N) experiment shows little change of

the boundary layer entropy in the deep convective region, consistent with minor change of monsoon circulation following desertification (from 15°N).

Another experiment was performed to isolate the relative roles of albedo and water availability changes. This experiment is identical to the standard deforestation experiment we just described in surface albedo but the water availability is fixed to that of the control experiment. The net surface radiative flux for this experiment is compared to those of the standard deforestation experiment and the control experiment (Fig. 16). The difference between this experiment and the control state is the net effect of the increasing surface albedo, whereas the difference between this experiment and the standard deforestation experiment indicates the net effect of the decreasing surface water availability. In terms of the relative contribution to the net surface radiation, we see that the effect of the surface moisture availability is substantial, although slightly smaller than the albedo effect here. The effect of decreasing surface water availability can explain almost completely the change in the longwave component of net radiation, whereas the effect of increasing surface albedo is responsible for the change in the shortwave component (Figs. 17 and 18).
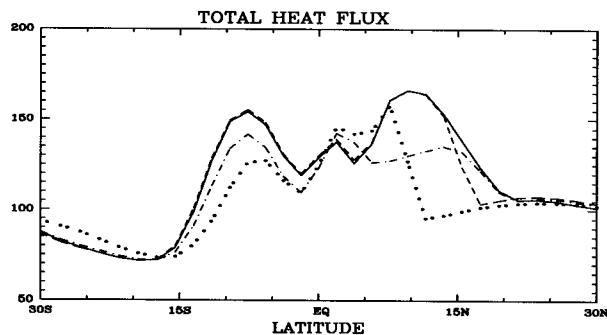

FIG. 15. The total surface fluxes (W m^{-2}) for the control (solid line), desertification from 15°N (dashed line), deforestation (dashed–dotted line), and desertification from 10°N (dotted line).
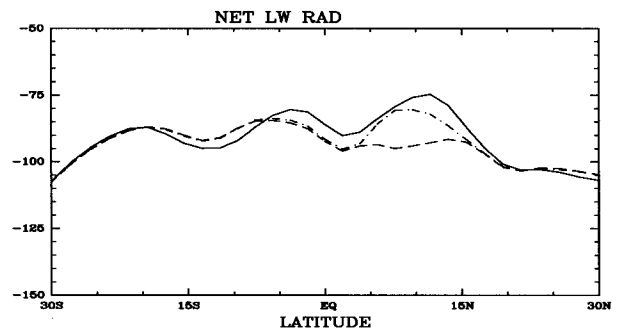

FIG. 17. Same as Fig. 16 but for the net surface longwave radiation. Note that the net surface longwave radiation is the downward longwave radiation emitting from the atmosphere less the upward longwave radiation emitting from the surface. Negative values indicate that the former is smaller than the latter in terms of magnitude.
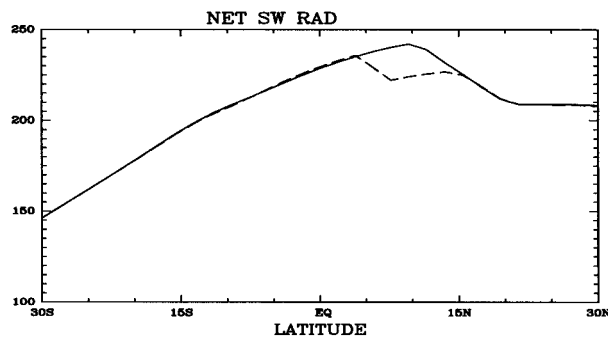
FIG. 18. Same as Fig. 16 but for the surface downward shortwave radiation. Note that the standard deforestation experiment and our hypothetical experiment here have indistinguishable surface downward solar radiation due to identical albedo.
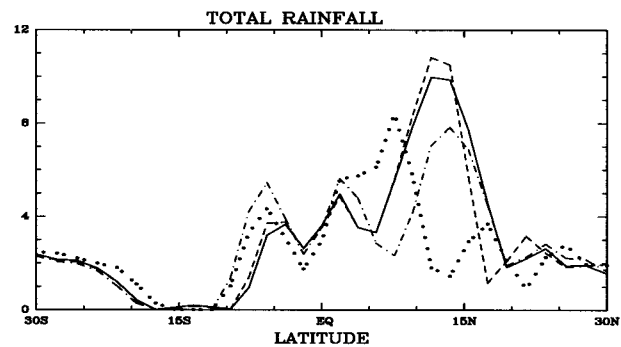

FIG. 19. The meridional distribution of rainfall in (mm day⁻¹), for the control (solid line), desertification (from 15° to 20°N, dashed line), deforestation (from 5° to 10°N, dashed–dotted line), and desertification (from 10° to 15°N, dotted line).

The model's result confirms our conceptual reasoning presented earlier and that of Eltahir (1996).

d. Desertification (from 10°N) experiment

The relation between the distribution of vegetation and the monsoon circulation is investigated further by considering the impact on the circulation that may result from desertification extending to 10°N. This experiment is identical to the control case except that we assign the value of the dryness index D to 3.0 (desert value) north of 10°N. As we can see from Fig. 8, the maximum rainfall occurs over the coastal region between about 6° and 8°N. Compared to both control and desertification (from 15°N) experiments, the rainfall belt (or ITCZ) has been pushed farther south. The region of the perturbation experiences strong negative moisture convergence and evaporation anomalies, resulting in substantial decrease of rainfall over that region. South of the perturbation region, we observe an increase of rainfall caused mainly by the increase of moisture convergence, similar to the desertification (from 15°N) case. In terms of the rainfall within Sahel region (~12°–18°N), where most previous studies were concerned, this case introduces the larger decrease compared to any other cases we described. The ITCZ stays over the coastal land and cannot move northward enough to bring rainfall to the Sahel region.

e. Other experiments

The distribution of vegetation that is shown in Fig. 4a is similar to the observed distribution over West Africa; the density of vegetation cover decreases from the south to the north. The areal extent of the three perturbations in vegetation cover are similar, each of them replaces the vegetation cover by a desert belt (for the deforestation experiment, a savanna belt) that extends for about 10° latitude. However, due to the different densities of the vegetation that existed initially at the three different locations, the intensities of the three per-

turbations are different. For example, the desertification (from 15°N) in fact only replaces the vegetation cover of 5° in width (from 15° to 20°N) by the desert. In order to test the robustness of our results, the same four experiments were repeated assuming that the distribution of vegetation in the control case is a uniform coverage by tropical forests (of course now the control case does not bear very much resemblance to reality). The results were not affected to any significant degree; that is, the model response is still sensitive to the location of the vegetation perturbation.

Clearly the model's quantitative response to the vegetation perturbation has to do with the latitudinal width as well as the magnitude of the perturbation. Here we conduct two experiments that correspond to the standard deforestation and desertification (from 10°N) experiments (Figs. 4c and 4d), respectively. The only difference is that the areal extent of the perturbation is now 5° instead of 10°. For the deforestation experiment, the perturbation is from 5° to 10°N (assigning dryness index the same as the standard deforestation experiment 1.75). For the desertification experiment, the perturbation is from 10° to 15°N with all the vegetation cover replaced by desert (i.e., $D = 3.0$).

The total rainfall for experiments with perturbations of 5° latitudinal width is shown in Fig. 19. The deforestation (from 5° to 10°N) experiment still shows substantial decrease of rainfall everywhere over the land area. However, the magnitude of rainfall decrease is smaller compared to the standard deforestation (from 5° to 15°N) experiment. In this case, it seems that a somewhat weaker monsoon circulation still exists. The ITCZ is pushed slightly northward. The desertification (from 10° to 15°N) experiment, on the other hand, shows a similar dramatic decrease of rainfall within the perturbation region. The ITCZ again is pushed southward to be around 6°–8°N.

Other experiments using different magnitudes of vegetation perturbation have also been performed to examine the robustness of our results. Although quantitative differences exist as we expect, the experiments

in general suggest that tropical deforestation is capable of producing substantial regional rainfall decrease over West Africa, just as the sub-Saharan desertification. In addition, it seems that the dynamics of West African monsoons are more susceptible to the vegetation cover near the tropical coastal region than that near the southern desert border. In what follows, we will summarize the results of the experiments we described and point out some important implications.

5. Discussion

The results of the numerical experiments of the previous section shed some light on the role of vegetation in the dynamics of West African monsoons. The vegetation cover along the coast of West Africa influences the simulated monsoons more significantly than vegetation cover near the desert border (north of 15°N). It is interesting to compare the response of the model to deforestation and desertification. Given the limitations of the model, the results of this exercise should be interpreted carefully, especially in comparison with the dynamics in the real atmosphere. However, comparison of the results for the different cases considered suggests that the dynamics of the monsoon in this region are indeed more sensitive to changes in land cover that may occur along the coast (deforestation, Fig. 4a) than changes in land cover that occur at the desert border (desertification, Fig. 4b).

These results are particularly interesting if we consider them in conjunction with the observed patterns of land cover change in West Africa. This region has been experiencing very intense changes in land cover throughout this century. The nature of land cover change in West Africa varies from desertification at the northern border to deforestation at the southern border. These changes in land cover are driven primarily by the increase in population. The demand for agricultural land is satisfied by clearing of natural vegetation, and the quality of vegetation cover is degraded by overgrazing in several regions. The timber industry flourishes along the coast of the Atlantic Ocean at the expense of continuous clearing of vast areas of the humid forests. The dry woodlands are popular sources of wood for domestic use. The combination of all these factors drives some of the most intense changes of land cover compared to any other region.

During the early years of this century, rain forests covered a significant area, about 500 000 km², along the Atlantic coast. Today, less than 10% of the primary rain forest is left. These estimates of tropical deforestation in West Africa were reported in Gornitz (1985) and Myers (1991). The highest annual rates of deforestation are in the Ivory Coast, Nigeria, and Ghana. The study of Myers (1991) estimates that the current annual rate of deforestation is 16% for Ivory Coast and 14% in Nigeria. Indeed, these are the highest annual rates of deforestation in the world. These estimates led Myers

(1991) to conclude that little primary forest is likely to be left in West Africa by about the year 2000.

Charney (1975) proposed a mechanism for describing the feedbacks between desertification and droughts. This theory is based on the basic concept that deserts work as radiative sinks of heat where the loss of heat due to the emission of planetary radiation is balanced by adiabatic warming due to subsidence. Under these conditions, removal of vegetation, such as that caused by overgrazing at the desert border, increases surface albedo causing an additional radiative cooling. The latter can only be balanced by additional adiabatic warming and enhancement of sinking motion. Charney (1975) argued that this enhancement of the sinking motion could push the ITCZ southward. While our simulations for the desertification case show anomalous sinking motion, the decrease of rainfall over the new desert is associated with changes in $P - E$ (circulation change) and a decrease in evaporation (local effect); see Figs. 8, 9, and 10. These kind of feedbacks cannot be addressed in the dry model of Charney (1975).

The same classic paper by Charney (1975) argues that, ''To my knowledge we do not yet have an explanation for the location of the ITCZ over the African continent, nor do we understand the nature of its interaction with the desert circulation.'' However, the simulations described in the previous section may shed some light on the dynamics of the monsoon circulation and the factors that govern the movement of the ITCZ onto the African continent. These results suggest that the distribution of vegetation plays a significant role in these processes. In particular, the type of vegetation that occupies the coastal region is important to the movement of the ITCZ onto the African continent. The mechanism by which vegetation in this zone interacts with the atmospheric circulation can be described by the theory of Eltahir (1996). Vegetation in the form of dense forests enhances net radiation at the surface, and the total flux of heat including sensible and latent forms. These fluxes supply energy as well as entropy in the boundary layer and create a significant gradient of entropy between land and ocean, which is the driving force for the monsoon circulation. The deforestation experiment illustrates how the removal of this vegetation would weaken the boundary layer entropy within the deep convective region and thus weaken the monsoon circulation and cause less rainfall over West Africa. For some extreme cases, like the vegetation perturbation we assumed in Fig. 4c, the monsoon can collapse as shown in Fig. 8. Figure 12 indicates that the radiative flux (therefore the entropy flux) decreases substantially over the perturbed region. For the case of the deforestation from 5° to 15°N, the total heat flux over the coastal region happens to be smaller than the oceanic value causing the collapse of the monsoon.

A comparison of the results of the four primary numerical experiments would suggest that the location of the simulated ITCZ is rather insensitive to the distri-

bution of vegetation northward (to a lesser extent southward) relative to the location of the ITCZ in the control experiment. In the desertification (from 15°N) experiment, although the magnitude of local rainfall is reduced relative to the control case, the location of the ITCZ does not change significantly compared to the control case. The same can be said in describing the deforestation (from 5° to 10°N) experiment. However, in the other experiments that involved changes in vegetation distribution within the vicinity of the ITCZ in the control experiment, the location of the ITCZ changes dramatically. This has important implications for GCM studies regarding effects of land surface transformation on the location of the ITCZ. That is, the response of different models to the same specified vegetation perturbation (e.g., desertification, which is the topic for most previous studies) might be different simply because different models have different control states. In general, for sub-Saharan desertification (degradation of the vegetation cover starts from the desert border southward), if the ITCZ for the control experiment lies within the region of perturbation, we expect a southward shift of the ITCZ as in the desertification (from 10°N) experiment, similar to the result of Xue and Shukla (1993). On the other hand, if the region of perturbation lies north of the ITCZ for the control case, we do not expect substantial change in the ITCZ position as in the desertification (from 15°N) experiment we have shown above. As far as deforestation (degradation of the vegetation cover starts from the coast northward) is concerned, the deforestation from 5° to 10°N has a tendency to push the ITCZ northward. For the worst-case scenario of deforestation (from 5° to 15°N), the monsoon collapses. The dynamics of West African monsoons seem to depend more on the vegetation cover from the location of the ITCZ (for the control run) southward than that from the location of the ITCZ (for the control run) northward.

In particular, we have shown that tropical deforestation may be a potentially important factor in modulating West African rainfall variability. This study suggests that tropical deforestation may be another possible drought-producing mechanism in West Africa besides the well-documented sub-Saharan desertification proposed first by Charney (1975). According to Nicholson (1994), 1950–69 were relatively wet years in Sahel and 1970–90 were relatively dry years. From the data of Nicholson (1994), we plot out the latitudinal distribution of the difference between normalized rainfall departures in West Africa in the dry (1970–90) and the wet (1950–69) periods. It is very clear that for the period of 1970–90 the rainfall is relatively low compared to the period 1950–69 over the whole West Africa (Fig. 20). Shinoda (1990) and Janicot (1992) analyzed the observed rainfall anomaly patterns over West Africa. They showed that droughts in the Sahel can be differentiated into those years with drought throughout the West African region and those with a dipole pattern with wetter than usual
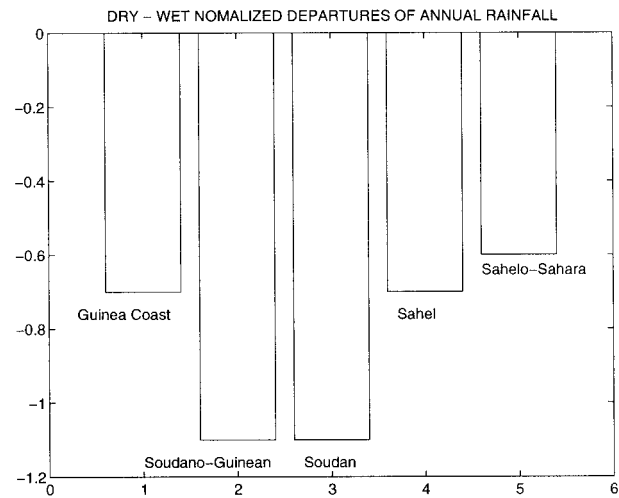

FIG. 20. The difference of normalized annual departures of African rainfall between the wet period of 1950–69 and the dry period of 1970–90 for different West African regions (dry–wet). The five regions are Guinea coast (1), Soudano–Guinean (2), Soudan (3), Sahel (4), and Sahelo–Sahara (5), as defined in Nicholson (1994).

conditions along the Guinea coast. While some years were associated with a southward shifting of the ITCZ accounting for a dry Sahel/wet Guinea coast, most of the Sahel drought years were dry throughout all of West Africa. As a result, the observations in Fig. 20 indicate that for the last three decades or so, all of West Africa experienced a deficit in rainfall. If the actual rainfall variability has anything to do with the land surface transformation (which may not be the case since SST could be another factor among others), Fig. 20 favors the role of deforestation since the effect of desertification on West African rainfall presents a dipole pattern (positive deviation south of the perturbation region and negative within the perturbation region; see Fig. 8), whereas the deforestation creates a universally negative deviation over the whole West Africa.

Furthermore, the basic difference between desertification near the desert border and deforestation near the coastal region is that the regrowth of grass is much easier than the regrowth of forest. While human activities (such as overgrazing) may easily cause desertification near the desert border, the natural variability of the whole climate system makes the recovery of the grassland possible by bringing more rainfall (for other reasons). The timescale for the regrowth of the grassland is on the order of months. It is then unlikely that the desertification is responsible for the long-lasting (decades) deficient rainfall over the Sahel. On the other hand, the tropical forest, once deforested, is much harder to recover. The timescale for recovery is years to several decades. Therefore, it is more likely that tropical deforestation may be responsible for a long-term rainfall variability, such as the decadal timescale drought near the Sahel region.

Recent studies have identified a strong link between

interannual Sahel rainfall anomalies and Atlantic intense hurricane activities (e.g., Gray 1990; Landsea and Gray 1992; Goldenberg and Shapiro 1996). Deficient Sahel rainfall corresponds to fewer U.S. east coast landfalls of intense Atlantic hurricanes since easterly waves originating from West Africa are the source of Atlantic hurricanes. If deforestation along the Guinea coast is responsible for the Sahel long-term rainfall decreases, it would follow that the cause of reduced numbers of intense Atlantic hurricanes during the 1970s through the early 1990s (Landsea et al. 1996) may be due to the deforestation along the Guinea coast.

We have to caution that there is little empirical evidence regarding the effect of land cover transformation on the West African monsoons (Nicholson 1988). Most studies on the impact of land cover modification on West African monsoons are based on models. In order to get significant response due to land cover change, large perturbation of the land surface properties (e.g., surface albedo) has been assumed. The magnitude of the perturbation is often unjustified. This is the main caveat of all the modeling studies (including this study). Nevertheless, this study shows the critical importance of the location of the vegetation perturbation in the dynamics of West African monsoons.

6. Conclusions and remarks

From the discussion we presented above, we can conclude the following.

1) Several numerical experiments were performed using a zonally symmetric model of the atmosphere with the vegetation distribution described by a simple parameterization. The objective of these experiments is to investigate the role of vegetation distribution in the atmospheric dynamics of West African monsoons and to determine how the atmosphere responds to changes in the lower boundary conditions. The results of the experiments suggest that the meridional distribution of vegetation plays a significant role in the dynamics of West African monsoons. The response of the atmosphere to any perturbation in the distribution of vegetation depends critically on the location of this perturbation.

2) Changes in vegetative cover along the border between the Sahara Desert and West Africa (desertification) leave a minor impact on the simulated monsoon circulation. These changes merely reduce the amount of rainfall at the desert border and slightly increase rainfall along the coast, but a healthy monsoon circulation still develops over the region.

3) Changes in vegetative cover along the southern coast of West Africa (deforestation) have a dramatic impact on the simulated atmospheric response. Deforestation excites a significant response in the model atmosphere and results in the collapse of the monsoon circulation for the worst-case scenario. The

physics of this response can be described by the mechanism of Eltahir (1996) with deforestation resulting in reducing surface net radiation, total flux of heat from the surface, and hence reducing boundary layer entropy. The response of the simulated monsoon circulation to the reduction of boundary layer entropy is consistent with the observations and theories of Eltahir and Gong (1996), Plumb and Hou (1992), and Emanuel (1995). Coastal deforestation is suggested as another drought-producing mechanism in West Africa besides well-documented desertification.

4) While the magnitude of local rainfall is sensitive to changes in local vegetation, the location of the ITCZ is not sensitive to changes in the vegetation northward or southward from the location of the ITCZ (control case). However, the location of the ITCZ is sensitive to changes in the distribution of vegetation in the immediate vicinity of the location of the ITCZ (control case).

The results of the numerical simulations shed some light on the relation between the dynamics of West African monsoons and the distribution of vegetation. However, extension of these results to describe the response of the real atmosphere to changes in the distribution of vegetation should be approached carefully due to the limitations of this simple model. In particular, the model was not designed to simulate the three-dimensional aspects of the relevant atmospheric dynamics. In reality, easterly waves are the rain-producing systems during the West African summer monsoon season. However, the life cycle of these disturbances is several days. Since we are mainly concerned with monthly to seasonal rainfall variability, we only care about the collective effect of these synoptic systems. The zonally symmetric model we use here should be sufficient for this purpose. A similar approach has been adopted by some previous studies. For example, Webster and Chou (1980) used a zonally symmetric model to simulate the seasonal structure of the Indian monsoon successfully although the rainfall in the actual Indian monsoon is associated with monsoon depressions, which are synoptic disturbances with a life cycle of several days.

It should also be noted that the model used here does not include cloud–radiation feedback. However, the qualitative effect of cloud–radiation is not hard to assess. Changes of net surface radiation due to vegetation degradation consist of the change in net solar radiation and the change in net terrestrial radiation, as we have seen in section 4. For the solar component, the vegetation degradation decreases cloudiness and thus allows more incoming solar radiation. This process works against the increase of surface albedo (which tends to reduce the net solar radiation at surface) following vegetation degradation. Therefore, the inclusion of cloud–radiation feedback tends to cancel the effect of surface albedo. Therefore, we expect less de-

crease of net solar radiation when cloud–radiation feedback is incorporated than otherwise. On the other hand, less cloudiness permits more longwave radiation to escape into outer space and results in a greater decrease of net surface longwave radiation. In short, the inclusion of cloud–radiation feedback may change the relative contribution to net surface radiation from shortwave and longwave components; that is, there is a greater decrease of net surface longwave radiation and a smaller decrease of net surface shortwave radiation following vegetation degradation. For example, Nobre et al. (1991) estimated a 26 W m^{-2} decrease of net surface radiation following a deforestation of large areas ($\sim10^6$ km^2) in Amazon. The decrease is composed of an 18 W m^{-2} decrease in net shortwave radiation and a 8 W m^{-2} decrease in net longwave radiation. No cloud–radiation feedback was included in this study. The study of Dickinson and Kennedy (1992) did include cloud–radiation feedback in its model. They reported an 18 W m^{-2} decrease of net surface radiation, for a similar area of deforestation. Of the total decrease of net surface radiation, now only 3 W m^{-2} comes from the decrease in net solar radiation; the other 15 W m^{-2} contribution is due to the decrease in net longwave radiation. We see clearly that even with the inclusion of cloud–radiation feedback, the net surface radiation still decreases following vegetation degradation although the magnitude is smaller, at least from these numerical model studies. Lean and Rowntree (1993) also reached a similar result to that of Dickinson and Kennedy (1992); again cloud–radiation feedback was included. The decrease is now mainly due to the decrease of net longwave radiation. Based on these considerations, we believe the essential results of this paper still hold true although quantitative differences should be expected.

Finally, the model land surface scheme may be too simple quantitatively. A more sophisticated land surface scheme should be helpful in simulating the land surface processes (e.g., surface evaporation) more accurately. In summary, this study represents the first step toward understanding the role of vegetation in the dynamics of West African monsoons. Our current research endeavors to relax the limitations mentioned above by using a three-dimensional regional climate model (e.g., Giorgi et al. 1993a, b).

APPENDIX

A Comparison of the Model Meridional Circulation with that of the NCEP Reanalysis

The model used in this study is designed as a process model. Therefore, only a limited set of physical processes is included. Although we do not expect this simple model to match the observations in the details, the model should capture the gross features of the observed monsoon circulation. The NCEP reanalysis 13-yr climatology (1982–94) (Kalnay et al. 1996) is used here as the "observations." We compare the model August output (with seasonal radiative forcing) with the NCEP data. Note that the model (with seasonal cycle) August monthly average is not exactly the same as that described in section 4 (steady state) since now August is just a part of the model seasonal cycle. It is more appropriate to compare the results of model with seasonal-varying insolation with the observations. Our goal here is not to verify our model simulation but assess the differences between our model and the observations. Possible reasons for these differences are presented.
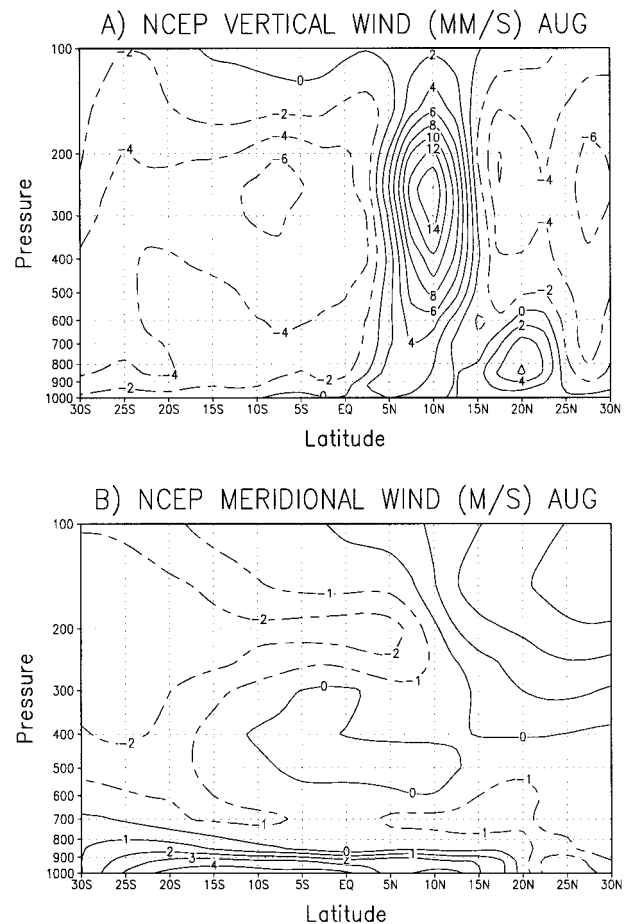

FIG. A1. The August (a) vertical wind (contour interval: 2 mm s^{-1}) and (b) meridional wind (contour interval: 1 m s^{-1}), averaged from 15°W to 15°E, for the NCEP climatology (1982–94).

A) MODEL VERTICAL WIND (MM/S) AUG

P — E (MM/DAY) AUG
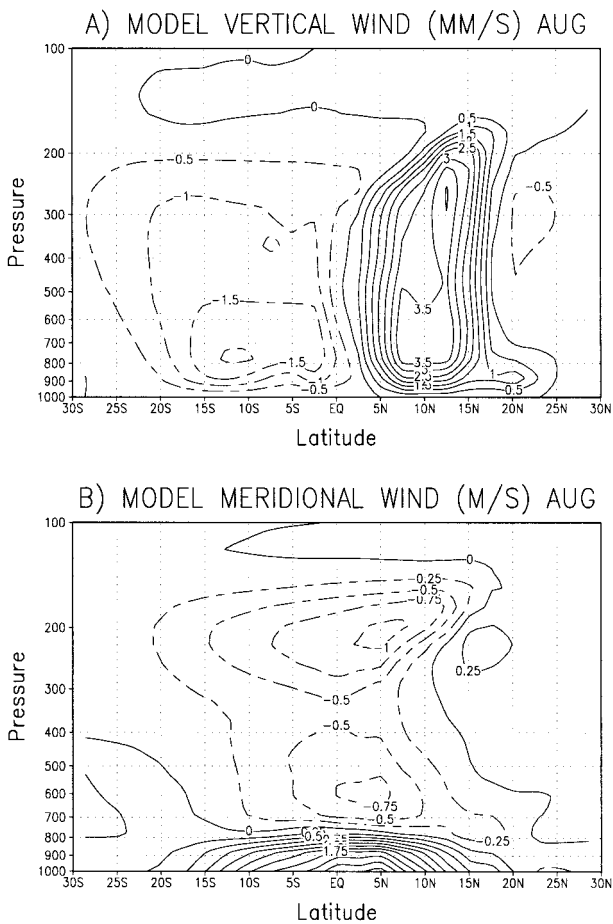
B) MODEL MERIDIONAL WIND (M/S) AUG

FIG. A2. The August (a) vertical wind (contour interval: 2 mm s^{-1}) and (b) meridional wind (contour interval: 1 m s^{-1}), averaged from 15°W to 15°E, for the model control run.

FIG. A3. The August precipitation minus evaporation in mm day^{-1}, a measure of moisture convergence. The solid line denotes the NCEP data and the dashed line denotes the model result.

Figure A1 shows the NCEP vertical and meridional winds averaged from 15°W to 15°E in August. Figure A2 shows the vertical and meridional winds for the model control experiment. The model captures the overall pattern of the overturning monsoon circulation, that is, the updraft centered around 10°N, the broad downdraft covering 5°N southward (Fig. A1a). Also consistent with the observation are the low-level southerlies and upper-level northerlies from 30°S to 20°N. On the other hand, the model results exhibit substantial quantitative deviations from the observations. Most notably, the vertical structure of the vertical and meridional winds in the model is different from the observations, especially the vertical wind. The observed monsoon circulation appears to be substantially stronger than that of the model. For example, the two downdrafts observed in the NCEP data (Fig. A1a) are evidently stronger than those in the model (Fig. A2a), particularly the one over the desert region (15°N northward). The updraft in the NCEP data also appears to be narrower than that in the model. All these suggest that the NCEP data show stronger monsoon circulations than those in the model. How-
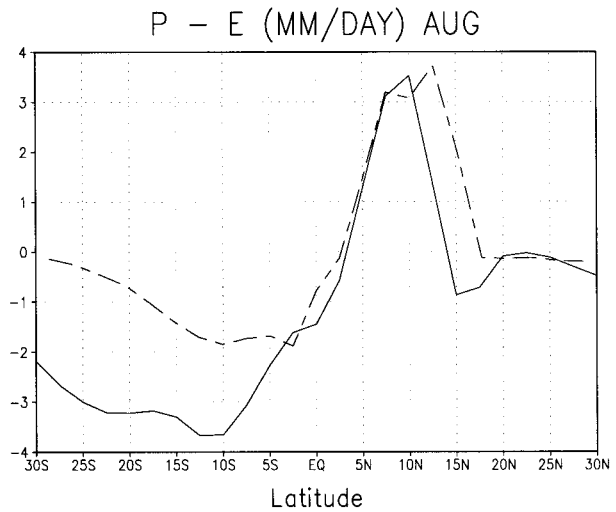
ever, the overall circulation patterns are simulated in our model, that is, the monsoon updraft near 10°N, the broad downdraft in the Southern Hemisphere, the weaker-than-observation downdraft over desert region. In addition, even though the model circulation is significantly weaker than that in the NCEP data, especially in the mid- and upper troposphere, the vertically integrated moisture convergence around the ITCZ is not very different (Fig. A3). This is probably because the moisture convergence is mainly determined by the low-level convergence of the monsoon circulation. The apparent larger-than-observed moisture convergence north of 10°N is consistent with the weaker-than-observed subsidence in that region. The clear difference in moisture convergence in the Southern Hemisphere is mainly due to the difference in evaporation, not in rainfall (not shown here).

The differences between the model output and the observations are not surprising. Take the vertical wind as an example. We know that the vertical wind is not a directly measured quantity, it reflects substantial influence from the NCEP model formulations (Kalnay et al. 1996). As the adiabatic cooling due to large-scale vertical motions is mostly balanced by diabatic heating in the Tropics, the vertical structure of vertical wind is dictated by that of the diabatic heating, mostly latent heating and radiative cooling. It follows that different parameterizations of moist convection and radiation would produce quite different vertical structure and intensity of large-scale motions. Moreover, the closure parameters of the Emanuel scheme we used are the cloud microphysical parameters; see section 3 for details. These parameters determine the convective heating and moistening. As discussed by Renno (1992), the convective heating and moistening are sensitive to these parameters. The parameters we used in this study follow

those of Emanuel (1991) and have not been validated against observations.

Finally, our adoption of zonal symmetry may also account for some of the differences in vertical wind. For example, Rodwell and Hoskins (1996) showed that the descent over desert region can be caused by the remote influence of Indian monsoon heating. They forced their three-dimensional model with a diabatic heating over the Indian continent. A descent over Sahara and a descent south of the equator were observed. These may explain why our model descents are substantially weaker than those of the NCEP data since our model does not include these mechanisms.

REFERENCES

Budyko, M. I., 1974: *Climate and Life.* International Geophysical Series, Vol. 18, Academic Press, 508 pp.

Charney, J. G., 1975: Dynamics of desert and drought in the Sahel. *Quart. J. Roy. Meteor. Soc.,* **101,** 193–202.

——, P. H. Stone, and W. J. Quirk, 1975: Drought in the Sahara: A biogeophysical feedback mechanism. *Science,* **187,** 434–435.

——, W. J. Quirk, S.-H. Chow, and J. Kornfield, 1977: A comparative study of the effects of albedo change on drought in semi-arid regions. *J. Atmos. Sci.,* **34,** 1366–1385.

Chou, M. D., 1984: Broadband water vapor transmission functions for atmospheric IR flux computations. *J. Atmos. Sci.,* **41,** 1775–1778.

——, and L. Peng, 1983: A parameterization of the absorption in the 15 μm CO_2 spectral region with application to climate sensitivity studies. *J. Atmos. Sci.,* **40,** 2183–2192.

——, D. P. Kratz, and W. Ridgway, 1991: Infrared radiation parameterizations in numerical climate models. *J. Climate,* **4,** 424–437.

Cunnington, C., and P. R. Rowntree, 1986: Simulations of the Saharan atmosphere-dependence on moisture and albedo. *Quart. J. Roy. Meteor. Soc.,* **112,** 971–999.

Dickinson, R. E., and P. Kennedy, 1992: Impacts on regional climate of Amazon deforestation. *Geophys. Res. Lett.,* **19,** 1947–1950.

Druyan, L. M., 1991: The sensitivity of sub-Saharan precipitation to Atlantic SST. *Climate Change,* **18,** 17–36.

Eltahir, E. A. B., 1992: Drought frequency analysis of annual rainfall series in central and western Sudan. *Hydrol. Sci. J.,* **37,** 185–199.

——, 1996: The role of vegetation in sustaining large scale atmospheric circulations in the tropics. *J. Geophys. Res.,* **101** (D2), 4255–4268.

——, and C. Gong, 1996: Dynamics of wet and dry years in West Africa. *J. Climate,* **9,** 1030–1042.

Emanuel, K. A., 1991: A scheme for representing cumulus convection in large-scale models. *J. Atmos. Sci.,* **48,** 2313–2335.

——, 1994: *Atmospheric Convection.* Oxford University Press, 580 pp.

——, 1995: On thermally direct circulations in moist atmospheres. *J. Atmos. Sci.,* **52,** 1529–1534.

——, J. D. Neelin, and C. S. Bretherton, 1994: On large-scale circulations in convecting atmospheres. *Quart. J. Roy. Meteor. Soc.,* **120,** 1111–1143.

Farmer, G., and T. M. L. Wigley, 1985: Climate trends for tropical Africa. Research Rep. for the Overseas Development Administration, 136 pp. [Available from Climate Research Unit, School of Environmental Sciences, University of East Anglia, Norwich NR4 7TJ, United Kingdom.]

Flohn, H., D. Henning, and H. C. Korff, 1965: Studies on the water-vapour transport over northern Africa. *Bonner Meteor. Abh.,* **6.**

Folland, C. K., T. N. Palmer, and D. E. Parker, 1986: Sahel rainfall and worldwide sea temperatures, 1901–85. *Nature,* **320,** 602–607.

Giorgi, F., M. R. Marinucci, and G. T. Bates, 1993a: Development of a Second-Generation Regional Climate Model (RegCM2). Part I: Boundary-layer and radiative transfer processes. *Mon. Wea. Rev.,* **121,** 2794–2813.

——, ——, and ——, 1993b: Development of a Second-Generation Regional Climate Model (RegCM2). Part II: Convective processes and assimilation of lateral boundary conditions. *Mon. Wea. Rev.,* **121,** 2814–2832.

Goldenberg, S. B., and L. J. Shapiro, 1996: Physical mechanisms for the association of El Niño and West African rainfall with Atlantic major activity. *J. Climate,* **9,** 1169–1187.

Gong, C., and E. A. B. Eltahir, 1996: Sources of moisture for rainfall in West Africa. *Water Resour. Res.,* **32,** 3115–3121.

Gornitz, V., 1985: A survey of anthropogenic vegetation changes in West Africa during the last century. *Climate Change,* **7,** 285–325.

Gray, W. M., 1990: Strong association between West African rainfall and US landfall of intense hurricanes. *Science,* **249,** 1251–1256.

Gutman, G., G. Ohring, and J. H. Joseph, 1984: Interaction between the geobotanic state and climate: A suggested approach and a test with a zonal model. *J. Atmos. Sci.,* **41,** 2663–2678.

Held, I. M., and A. Y. Hou, 1980: Nonlinear axially symmetric circulations in a nearly inviscid atmosphere. *J. Atmos. Sci.,* **37,** 515–533.

Horton, E. B., and D. E. Parker, 1997: Global and regional climate in 1996. *Weather,* **52,** 174–182.

Huffman, G. J., R. F., Adler, B. Rudoff, U. Schneider, and P. R. Keehn, 1995: Global precipitation estimates based on a technique for combining satellite-based estimates, rain gauge analysis, and NWP model precipitation estimates. *J. Climate,* **8,** 1284–1295.

Hulme, M., 1994: Century-scale series of regional rainfall anomalies in Africa. *Trends (93): A Compendium of Data on Global Change,* T. A. Boden et al., Eds., Carbon-Dioxide Information Analysis Center, Oak Ridge National Laboratory, 964–973.

Janicot, S., 1992: Spatio-temporal variability of West African rainfall. Part I: Regionalizations and typings. *J. Climate,* **5,** 489–497.

Joseph, J. H., W. J. Wiscombe, and J. A. Weinman, 1976: The delta-Eddington approximation for radiative flux transfer. *J. Atmos. Sci.,* **33,** 2452–2459.

Kalnay, E., and Coauthors, 1996: The NCEP/NCAR 40-year reanalysis project. *Bull. Amer. Meteor. Soc.,* **77,** 437–471.

Kidson, J. W., 1977: African rainfall and its relation to the upper air circulation. *Quart. J. Roy. Meteor. Soc.,* **103,** 441–456.

King, M. D., and Harshvardhan, 1985: Comments on ''The parameterization of radiation for numerical weather prediction and climate models.'' *Mon. Wea. Rev.,* **113,** 1832–1833.

Kitoh, A., K. Yamzaki, and T. Takiota, 1988: Influence of soil moisture and surface albedo changes over African tropical rainforest on summer climate investigated with MRI-GCM-I. *J. Meteor. Soc. Japan,* **66,** 65–85.

Kutzbach, J., G. Bonan, J. Foley, and S. P. Harrison, 1996: Vegetation and soil feedbacks on the response of the African monsoon to orbital forcing in the early to middle Holocene. *Nature,* **384,** 623–626.

Lacis, A. A., and J. E. Hansen, 1974: A parameterization for the absorption of solar radiation in the earth's atmosphere. *J. Atmos. Sci.,* **31,** 118–133.

Lamb, P. J., 1978a: Case studies of tropical Atlantic surface circulation patterns during recent sub-Saharan weather anomalies: 1967 and 1958. *Mon. Wea. Rev.,* **106,** 482–491.

——, 1978b: Large-scale tropical Atlantic surface circulation patterns associated with sub-Saharan weather anomalies. *Tellus,* **30,** 240–251.

——, 1983: West African water vapor variations between recent contrasting sub-Saharan rainy seasons. *Tellus,* **35A,** 198–212.

——, and R. A. Peppler, 1992: Further case studies of tropical Atlantic surface atmospheric and oceanic patterns associated with sub-Saharan drought. *J. Climate,* **5,** 476–488.

Landsea, C. W., and W. M. Gray, 1992: The strong association be-

tween western Sahel monsoon rainfall and intense Atlantic hurricanes. *J. Climate,* **5,** 435–453.

——, N. Nicholls, W. M. Gray, and L. A. Avila, 1996: Downward trends in the frequency of intense Atlantic hurricanes during the past five decades. *Geophys. Res. Lett.,* **23,** 1697–1700.

Lean, J., and P. R. Rowntree, 1993: A GCM simulation of the impact of Amazonian deforestation on climate using improved canopy representation. *Quart. J. Roy. Meteor. Soc.,* **119,** 509–530.

Lindzen, R. S., and A. Y. Hou, 1988: Hadley circulations for zonally averaged heating centered off the equator. *J. Atmos. Sci.,* **45,** 2416–2427.

Lough, J. M., 1986: Tropical sea surface temperature and rainfall variation in sub-Saharan Africa. *Mon. Wea. Rev.,* **114,** 561–570.

McClatchey, R. A., R. W. Fenn, J. E. A. Selby, F. E. Volz, and J. S. Garing, 1972: Optical properties of the atmosphere. Air Force Cambridge Research Laboratories Environmental Research Pap. 411.

Myers, N., 1991: Tropical forests: Present status and future outlook. *Climate Change,* **19,** 3–32.

Newell, R. E., J. W. Kidson, D. G. Vincent, and G. J. Boer, Eds., 1972a: *The General Circulation of the Tropical Atmosphere.* Vol. 1. The MIT Press, 258 pp.

——, ——, ——, and ——, Eds., 1972b: *The General Circulation of the Tropical Atmosphere.* Vol. 2. The MIT Press, 371 pp.

Nicholson, S. E., 1988: Land surface atmosphere interaction. *Prog. Phys. Geogr.,* **12,** 36–65.

——, 1994: Century-scale series of standardized annual departures of African rainfall. *Trends (93): A Compendium of Data on Global Change,* T. A. Boden et al., Eds., Carbon-Dioxide Information Analysis Center, Oak Ridge National Laboratory, 952–962.

——, M. B. Ba, and J. Y. Kim, 1996: Rainfall in the Sahel during 1994. *J. Climate,* **9,** 1673–1676.

Nobre, C. A., P. J. Sellers, and J. Shukla, 1991: Amazonian deforestation and regional climatic change. *J. Climate,* **4,** 957–988.

Owen, J. A., and M. N. Ward, 1989: Forecasting Sahel rainfall. *Weather,* **44,** 57–64.

Plumb, R. A., and A. Y. Hou, 1992: The response of a zonally symmetric atmosphere to subtropical thermal forcing: Threshold behavior. *J. Atmos. Sci.,* **49,** 1790–1799.

Ramage, C. S., 1971: *Monsoon Meteorology.* Academic Press, 296 pp.

Rasmusson, E. M., 1972: Seasonal variation of the tropical humidity parameters. *The General Circulation of the Tropical Atmosphere,* Vol. 1, R. E. Newell et al., Eds., The MIT Press, 193–221.

Renno, N. O., 1992: Moist convection parameterization and numerical modelling of moist atmospheres. Ph.D. thesis, Massachusetts

Institute of Technology, 297 pp. [Available from Massachusetts Institute of Technology, 77 Massachusetts Ave., Cambridge, MA 02139.]

Reynolds, R. W., and T. M. Smith, 1994: Improved global sea surface temperature analyses. *J. Climate,* **7,** 929–948.

Rodgers, C. D., 1968: Some extension and applications of the new random model for molecular band transmission. *Quart. J. Roy. Meteor. Soc.,* **94,** 99–102.

Rodriguez-Iturbe, I., D. Entekhabi, and R. L. Bras, 1991: Nonlinear dynamics of soil moisture at climate scales: 1. Stochastic analysis. *Water Resour. Res.,* **27,** 1899–1906.

Rodwell, M. J., and B. J. Hoskins, 1996: Monsoons and the dynamics of deserts. *Quart. J. Roy. Meteor. Soc.,* **122,** 1385–1404.

Rowell, D. P., and C. Blondin, 1990: The influence of soil wetness distribution on short range rainfall forecasting in the West African Sahel. *Quart. J. Roy. Meteor. Soc.,* **116,** 1471–1485.

Shinoda, M., 1990: Long-term variability of the tropical African rainbelt and its relation to rainfall in the Sahel and northern Kalahari. *J. Meteor. Soc. Japan,* **68,** 19–35.

Sud, Y. C., and M. J. Fennessy, 1984: Influence of evaporation in semi-arid regions on the July circulation: A numerical study. *J. Climatol.,* **4,** 383–398.

——, and A. Molod, 1988: A GCM simulation study of the influence of Saharan evapotranspiration and surface albedo anomalies on July circulation and rainfall. *Mon. Wea. Rev.,* **116,** 2388–2400.

Walker, J., and P. R. Rowntree, 1977: The effect of soil moisture on circulation and rainfall in a tropical model. *Quart. J. Roy. Meteor. Soc.,* **103,** 29–46.

Webster, P. J., and L. C. Chou, 1980: Seasonal structure of a simple monsoon system. *J. Atmos. Sci.,* **37,** 354–367.

Xue, Y., and J. Shukla, 1993: The influence of land surface properties on Sahel climate. Part I: Desertification. *J. Climate,* **6,** 2232–2245.

——, K. N. Liou, and A. Kasahara, 1990: Investigation of biogeophysical feedback on the African climate using a two-dimensional model. *J. Climate,* **3,** 337–352.

Yeh, T.-C., R. T. Wetherald, and S. Manabe, 1984: The effect of soil moisture on the short-term climate and hydrology change—A numerical experiment. *Mon. Wea. Rev.,* **112,** 474–490.

Zheng, X., 1997: Moist zonally-symmetric models and their applications to West African monsoons. Ph.D. thesis, Massachusetts Institute of Technology, 217 pp. [Available from Massachusetts Institute of Technology, 77 Massachusetts Ave., Cambridge, MA 02139.]

——, and E. Eltahir, 1997: The response to deforestation and desertification in a model of West African monsoons. *Geophys. Res. Lett.,* **24,** 155–158.

——, and ——, 1998: A soil moisture–rainfall feedback mechanism: 2. Numerical experiments. *Water Resour. Res.,* **34,** 777–785.